Can. J. Remote Sensing, Vol. 37, No. 5, pp. 564–582, 2011

The integration of optical, topographic, and radar data for wetland mapping in northern Minnesota

Jennifer Corcoran, Joseph Knight, Brian Brisco, Shannon Kaya, Andrew Cull, and Kevin Murnaghan

Abstract. Accurate and current wetland maps are critical tools for water resources management, however, many existing wetland maps were created by manual interpretation of one aerial image for each area of interest. As such, these maps do not inherently contain information about the intra- and interannual hydrologic cycles of wetlands, which is important for effective wetland mapping. In this paper, several sources of remotely sensed data will be integrated and evaluated for their suitability to map wetlands in a forested region of northern Minnesota. These data include: aerial photographs from two different times of a growing season, National Elevation Dataset and topographical derivatives such as slope and curvature, and multitemporal satellite-based synthetic aperture radar (SAR) imagery and polarimetric decompositions. We identified the variables that are most important to accurately classify wetland from upland areas and discriminate between wetland types for a forested region of northern Minnesota using the decision-tree classifier randomForest. The classifier was able to differentiate wetland from upland and water with 75% accuracy using optical, topographic, and SAR data combined, compared with 72% using optical and topographical data alone. Classifying wetland type proved to be more challenging; however, the results were significantly improved over the original National Wetland Inventory classification of only 49% compared with 63% using optical, topographic, and SAR data combined. This paper illustrates that integration of remotely sensed data from multiple sensor platforms and over multiple periods during a growing season improved wetland mapping and wetland type classification in northern Minnesota.

Résumé. Les cartes précises et à jour des milieux humides sont des outils essentiels pour la gestion des ressources en eau; toutefois, de nombreuses cartes des milieux humides existantes furent créées à l'aide de l'interprétation manuelle d'une seule image aérienne pour chaque zone d'intérêt. Comme tel, ces cartes ne contiennent pas d'information inhérente sur les cycles hydrologiques intra- et interannuels des milieux humides qui constitue une information essentielle pour la cartographie efficace des milieux humides. Dans cet article, diverses sources de données de télédétection seront intégrées et évaluées pour leur capacité à cartographier les milieux humides dans une région boisée située dans le nord du Minnesota. Ces données incluent : des photographies aériennes acquises à deux périodes différentes de la saison de croissance, un ensemble de données « National Elevation Dataset » et des dérivées topographiques comme la pente et la courbure, des images satellite multi-temporelles radar à synthèse d'ouverture (RSO) ainsi que des décompositions polarimétriques. On identifie les variables les plus importantes pour la classification précise des milieux humides par rapport aux zones de hautes terres et pour la détermination des types de milieux humides pour une zone boisée dans le nord du Minnesota à l'aide du classifieur randomForest basé sur un arbre de décision. Le classifieur a permis de différencier les milieux humides des hautes terres et de l'eau avec une précision de 75 % en utilisant une combinaison de données optiques, topographiques et radar comparativement à 72 % en utilisant des données optiques et topographiques uniquement. La classification des types de milieux humides s'est avérée plus difficile à réaliser; cependant, les résultats étaient significativement meilleurs par rapport à la classification originale du « National Wetland Inventory » qui était de seulement 49 % comparativement à 63 % en utilisant une combinaison de données optiques, topographiques et radar. Globalement, on montre dans cet article que l'intégration des données de télédétection multi-capteurs et sur des périodes multiples durant la saison de croissance peut améliorer la cartographie des milieux humides ainsi que la classification des types de milieux humides dans le nord du Minnesota.

Introduction

Wetlands are valuable ecosystems in many ways. For example, wetlands provide filtration of wastewater (Vymazal, 2005), groundwater recharge (van der Kamp and Hayashi, 1998; Acharya and Barbier, 2000), and water retention to reduce damages caused by flooding (Mitsch and Gosselink, 2000). Accurate wetland maps are important

Received 1 April 2011. Accepted 5 December 2011. Published on the Web at http://pubs.casi.ca/journal/cjrs on 16 March 2012.

Jennifer Corcoran[1] and Joseph Knight. University of Minnesota, Department of Forest Resources, 115 Green Hall, 1530 Cleveland Avenue N, St. Paul, MN 55108.

Brian Brisco, Shannon Kaya, Andrew Cull, and Kevin Murnaghan. Canada Centre for Remote Sensing, Natural Resources Canada, 588 Booth Street, Ottawa, ON K1A 0Y7, Canada.

[1]Corresponding author (e-mail: murph636@umn.edu).

for conservation and restoration efforts, and they are crucial for developing emergency response plans for natural disasters. For instance, in the Wild Rice River Watershed of the Red River Basin, which covers portions of the United States and Canada, agencies from two U.S. states, one Canadian province, and both national governments respond to the frequent and significant flood events on the Red River (Hearne, 2007). Though these agencies have different laws and methods for responding to extreme flooding, all require the most accurate and current water resource maps, and the techniques to create them, to assess and manage flood events.

A wetland map is a two-dimensional representation of a four-dimensional phenomenon (including space and time). Wetland boundaries are dynamic and fluctuate both inter- and intra-annually depending on many factors including rainfall, evaporation, ground water flow, and land use manipulation. Wetland inventories are important tools for managing and protecting wetlands. Therefore, the accuracy of wetland mapping methods is critically important for a broad range of water resource management concerns. Among these concerns are regulatory purposes such as permitting, mitigation, and monitoring compliance; monitoring of changes in wetland extent or function due to natural and anthropogenic causes; and selection of areas that have the most suitable hydrologic and vegetative characteristics for wetland restoration or conservation (Deschamps et al., 2002; Brooks et al., 2006; Hearne, 2007). Given the dynamic nature of wetlands, having access to a synoptic wetland inventory map is an important first step in making sound water resource management decisions.

The U.S. National Wetlands Inventory (NWI) from the U.S. Fish and Wildlife Services was not designed to show exact wetland boundaries, but rather to provide generalized boundaries and approximate locations in a snapshot of time (United States Fish and Wildlife Service, 2009). The U.S. Environmental Protection Agency called for achieving a net increase in wetland acres by 2011. Similarly, the State of Minnesota enacted the Wetland Conservation Act with a goal of "no net loss" in wetlands statewide. Both of the aforementioned goals require the continuous creation of robust maps of current wetlands and practical techniques for monitoring land use change impacts on wetlands over large geographical areas. Once presented with a reliable wetland inventory, water resource managers charged with accomplishing these regulatory goals can design adaptive management approaches to prioritize areas for conservation and restoration.

Traditional methods of mapping wetlands have relied on aerial photograph interpretation or classification of optical satellite imagery. However, such maps are typically based on single-date optical imagery, are often several years old, may not be representative of the current state of the environment, and do not take into account the dynamic nature of wetlands. One wetland type in particular that is problematic to map is forested wetlands. Separating forested wetlands from forested uplands with optical imagery is challenging because the imagery, even if collected during leaf-off conditions, may not reveal the underlying hydrology of a site. The collection of optical imagery can also be hindered by cloud cover, thus potentially missing the critical post-snow, leaf-off period for wetland inventory. Many wetlands are only flooded or saturated ephemerally, so those wetlands may not have been mapped in the original NWI (Dahl, 1990). Optical imagery may reveal these wetlands, if the timing of the imagery collection is perfect, but it is difficult to predict when that time is and to complete data acquisition during that time.

The addition of other remotely sensed data, such as radio detection and ranging (radar) data, can offer unique information about surface features beyond the radiometric response measured with optical data. This additional information can help to identify inundation (Hess et al., 2003; Frappart et al., 2005; Lu and Kwoun, 2008; Lane and D'Amico, 2010) and classify wetland areas (Touzi, 2006; Ban et al., 2010) based on surface structure and hydrologic features that may not otherwise be differentiable with aerial photography alone.

In certain areas and during periods of frequent cloud cover, optical wavelengths have an obvious disadvantage in that data cannot be acquired. Long-wave radar signals, on the other hand, are not sensitive to the atmosphere, do not require daylight hours for acquisition, and thereby increase the possibility for frequent data collection (Townsend, 2001; Parmuchi et al., 2002). In addition, polarimetric information from synthetic aperture radar (SAR) allows for the discrimination between different scattering mechanisms contributing to the overall backscatter in an image (Townsend, 2001; Parmuchi et al., 2002; Brisco et al., 2008). Polarimetric scattering signatures can be interpreted to identify landscape variables associated with the primary surface-scattering mechanism identified for each area through products known as polarimetric decompositions (Touzi et al., 2009).

Incorporating data from multiple sensor platforms and over multiple seasons will increase the likelihood of differentiating between a broader range of wetland types (Ramsey et al., 1995; Ozesmi and Bauer, 2002; Töyrä et al., 2002; Li and Chen, 2005; Castañeda and Ducrot, 2009; Ramsey et al., 2009; Bwangoy et al., 2010). By acquiring fully polarimetric SAR data from multiple dates over a season, the relative backscatter response from varying hydrologic periods and both leaf-on and leaf-off conditions can help determine the seasonality of wetlands and thus classify wetland types with higher accuracy. However, given the integration of such a large number of data inputs, it is important to determine the optimal set of data to reduce redundancy and increase the accuracy and efficiency of implementing mapping wetlands over large spatial scales, a goal that can be accomplished by decision-tree classification.

This study investigated how the accuracy of wetland mapping can be improved by integrating several sources of remotely sensed data, including: leaf-on and leaf-off high resolution aerial orthophotos, National Elevation Dataset

(NED) and topographic derivatives, and fully polarimetric RADARSAT-2 imagery. We address the following hypotheses: (*i*) seasonal fully polarimetric SAR imagery provides important information about surface scattering mechanisms, allowing more accurate distinction of wetland type; and (*ii*) the integration of optical, topographic, and SAR data using a decision-tree classifier provides a more accurate method for wetland mapping and classifying specific wetland types.

Methodology

Study site

This research focused on improving wetland classification accuracy, in particular the classification of forested wetlands in northern Minnesota. Minnesota is rich with geological history, containing volcanic and sedimentary rocks from millions of years ago. Much of the state has been carved by several glacial advances and retreats over the millennia, leaving glacial deposits, lakes, and rivers in their wake (MN DNR, 2011). Northeastern Minnesota, otherwise known as the Arrowhead, is a region currently dominated by hardwood and conifer forests, as well as woody and herbaceous wetlands (USDA-NASS, 2011). This region is sparsely populated, with the exception of a few larger cities near Lake Superior, namely Cloquet and Duluth, with populations of 12 124 and 86 265 in 2010, respectively (AdminMN, 2011). The chosen study site centered on Cloquet, Minn. is generally representative of the land cover characteristic of the Arrowhead region (**Figure 1**). The elevation in this study site ranges from about 330–450 m above sea level (mean of 392 m) and the slope of the landscape is on average less than 1.7°.

Classification schemes

Two classification schemes were used in this paper, including a simple upland/water/wetland determination and a modified version of the Cowardin classification (Cowardin, 1979). The modified Cowardin classification scheme involved reclassifying the following classes: flooded and intermittent lakes, unconsolidated bottom water bodies, and rivers merged into one "water" class; aquatic bed and emergent wetlands merged into "emergent wetlands"; "forested wetlands" and "scrub/shrub wetlands" remained the same; and all nonwetland areas were initially separated into "agriculture", "forest", "grassland", "rural", and "urban" classes for training the decision-tree classifier, then later merged into one "upland" class. The simple upland/water/wetland determinant classification was based on appropriate consolidation of the aforementioned upland and Cowardin wetland classes.

Field data

Multiple sets of field data were used in this research, including field point data collected in the summers of 2009 and 2010 and the MN DNR Wetland Status and Trends Monitoring Program (WSTMP) polygons from 2006–2008 (**Table 1**). The WSTMP polygons were created by randomly distributing 4990 one-square-mile primary sampling units (PSUs) statewide, divided into three panels. One panel was photographed with spring leaf-off (or early leaf on-set) high-resolution aerial photography each year and the PSUs were digitized using a Cowardin classification scheme by trained photo interpreters. The initial digitized polygons were then reviewed by a second team of senior photo interpreters and a subset of the PSUs was field-verified and used to evaluate

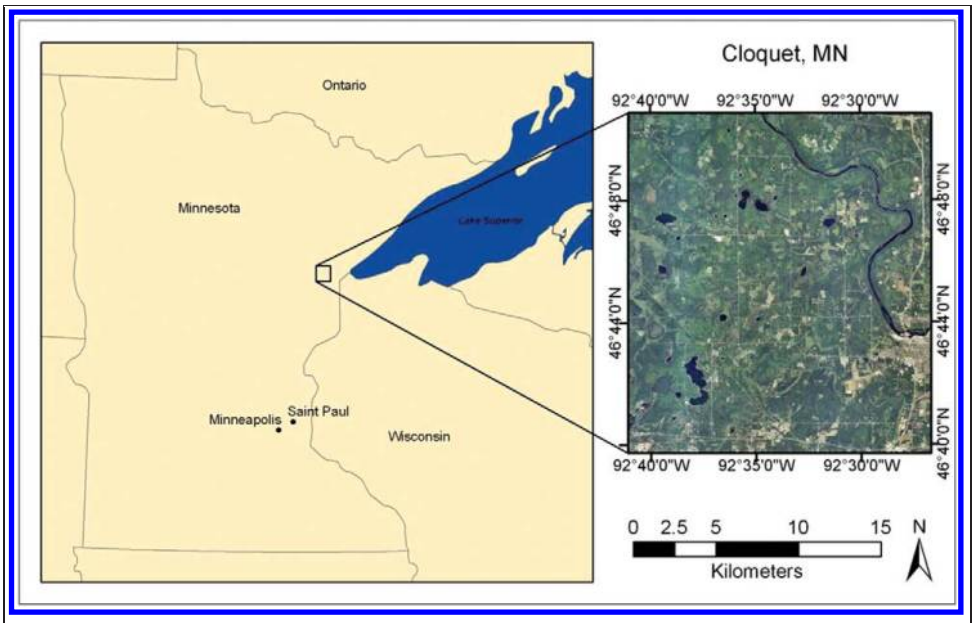

Figure 1. Study area for this project, near Cloquet, MN. Inset image was created using the aerial orthophoto from summer 2008 as a background.

the accuracy of each panel. A general 30% rule was followed while digitizing the WSTMP polygons, in which if a land class appeared to occupy more than 30% of the polygon, then it was designated as that class. An exception to the 30% rule was where more than one class of vegetation existed; in this case, the taller plant class took precedence (MN DNR, 2010). The centroids of WSTMP polygons were used in addition to the field point data collected in 2009 and 2010.

The field data collection protocol for 2009 and 2010 involved the following: locating and physically visiting ground reference points with a GPS unit; recording the position with a minimum of 50 GPS fixes; identifying the dominant wetland type using the Cowardin classification scheme (Cowardin, 1979); taking representative photographs using the built-in camera on the GPS unit; and recording the point ID, description, and spatial coordinates in a field notebook for back-up purposes. In addition to the 2009, 2010, and WSTMP training data, additional points were added using manual photo interpretation to ensure a suitable distribution of points per class.

Decision-tree classification

A decision-tree classification approach provides an efficient means of establishing relationships between dependent and independent variables using training data, such that predictions can be repeatedly and robustly made of unclassified datasets (Hogg and Todd, 2007). Several decision-tree classification software programs are available, each having strengths and weaknesses regarding usability, accuracy, and performance (Ruefenacht et al., 2008). The decision-tree classifier randomForest was used in this research and was run using the R Statistical Package module within Python. RandomForest was chosen for this research because of the robustness of the results, ease and speed of use, and the ability to produce confidence maps of the classification results. Programming code was provided by the U.S. Department of Agriculture (USDA) Forest Service Remote Sensing Applications Center (Ruefenacht et al., 2008) to generate an output classification and associated confidence map, while R was used to compute summary statistics and figures about the classification results.

A stratified random sample of 75% of the field data was used to train the decision-tree classifier, while the remaining 25% were used as a reference dataset to independently assess the accuracy. For a summary of the number of points available per land class for training and accuracy assessment, see **Table 1**. Two decision trees were built per classification scheme, the first using optical and topographical data alone, the second using a combination of optical and topographic data as well as all available SAR data (including two dates of backscatter from four polarizations and four dates of three different polarimetric decompositions).

Table 1. Summary of decision-tree classifier training points and independent tests points for accuracy assessment of the results.

	No. of points		
Land Cover Classification	Training	Test	Total
Upland–wetland determinant			
Upland	464	152	616
Water	69	23	92
Wetland	421	140	561
Total	954	315	1269
Modified Cowardin class			
Water	69	23	92
Emergent wetland	97	37	134
Forested wetland	156	48	204
Scrub/shrub wetland	168	55	223
Upland	464	152	616
Total	954	315	1269

Datasets

Optical and topographical

Two periods of high-resolution aerial orthophotos were used in this research, including: 2008 mid-summer (full canopy, 1 m resolution) and 2009 spring (early leaf onset, 50 cm resolution) imagery (**Figure 2**). Both sets of imagery were acquired with color and near infrared bands. **Figure 3** shows the response signature, or frequency diagram, of the brightness values in each optical band at two different times for upland and wetland classified reference field sites. The decision-tree classifier will attempt to capitalize on the spectral differences between the land class types in each optical band. Rooted in the wetland response signatures are the response signatures of each wetland class, shown in **Figure 4**. There were noticeable differences between emergent wetlands and forested or scrub/shrub wetlands, particularly in the responses from early leaf-onset period of the 2009 aerial orthophotos. For example, there was a high frequency of low brightness values in emergent wetlands in the 2009 orthophoto, this could be due to wetter soils and more plants absorbing light and reflecting less. There was also a higher range of values in each band of the 2009 orthophoto for emergent wetlands compared to forested or scrub/shrub wetlands, this is likely due to emergent wetlands having more variety of plant species, wetness, and patches of exposed bare soil.

The 2008 aerial photography was acquired as a part of the USDA Farm Service Administration National Agricultural Imagery Program and was found to have a horizontal accuracy of 2.66 m (MnGeo, 2011). The 2008 imagery were downloaded by county from the USDA Geospatial Data Gateway, mosaicked, and clipped. The spring early leaf-onset aerial photography was provided by the MN DNR and acquired as a part of a collaboratively funded program between several state and federal agencies, including the MN DNR, MN Pollution Control Agency, and U.S. Geological Survey (USGS). All bands from each date of aerial orthophotos were used in the decision-tree

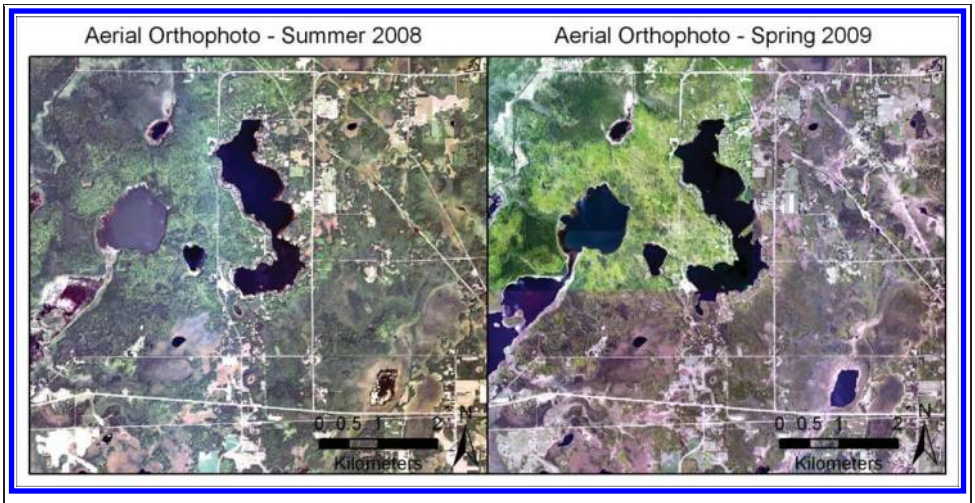

Figure 2. Two different time periods of aerial orthophoto imagery were used in the decision-tree classifier: full canopy in mid-summer 2008 and early leaf-onset in spring 2009. This subset area illustrates how the imagery for 2009 was collected at different times during the spring.

classification. In addition, the red and near infrared bands were used to calculate normalized difference vegetation index (NDVI) (Campbell, 2007). Because of a requirement of the decision-tree algorithm utilized in this research, the imagery was degraded to mimic the minimum resolution (10 m) of all concurrent input datasets (**Figure 5**).

Wetlands tend to be located in low-lying or depressional areas on the landscape. Therefore, the USGS NED was

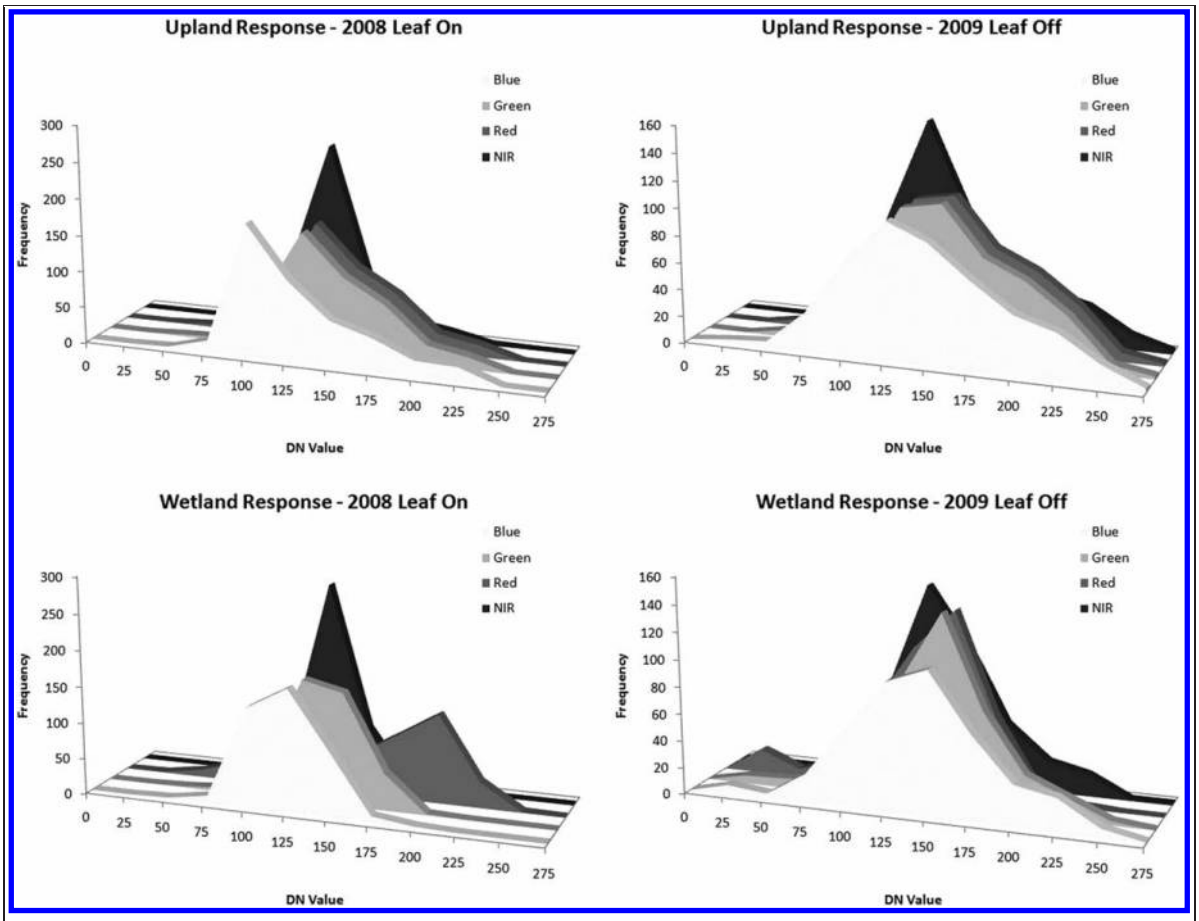

Figure 3. Spectral response signatures for each of the optical bands extracted from field reference data points of upland and wetland class categories and for each source of aerial orthophoto, summer 2008 and 2009 early leaf-onset.

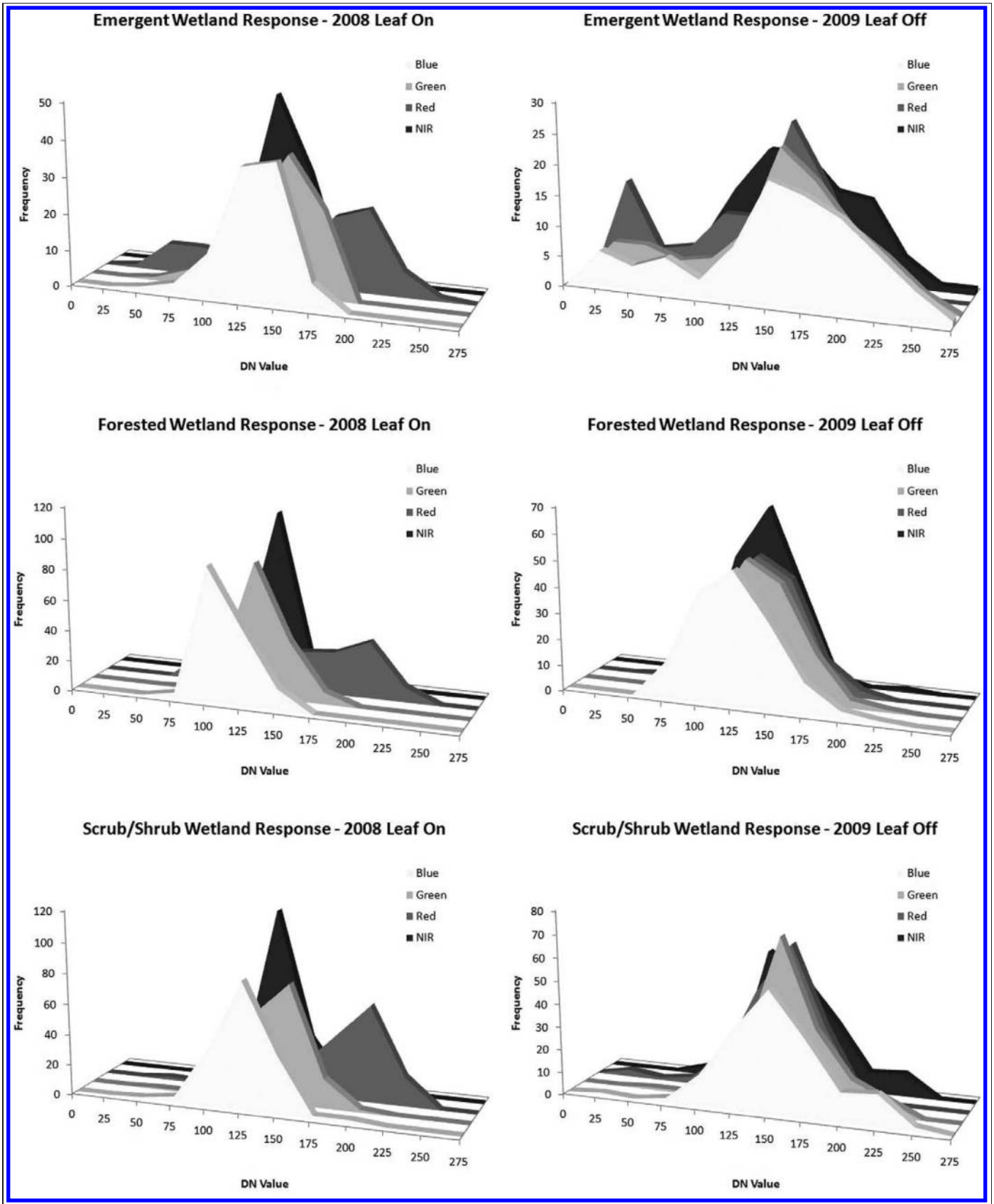

Figure 4. Spectral response signatures for each of the optical bands extracted from field reference data points of emergent, forested, and scrub/shrub wetland class types and for each orthophoto source: summer 2008 and 2009 early leaf-onset.

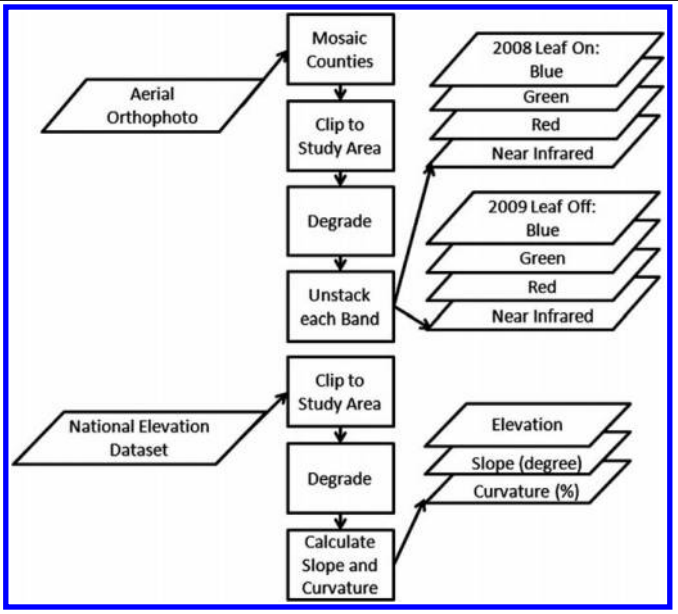

Figure 5. Optical and topographic input data, preprocessing methods, and output data for decision-tree classification.

obtained for the study area. The NED is available at 1/3 Arc Sec, or 10 m resolution, and was similarly downloaded by county from the USDA Geospatial Data Gateway, mosaicked, clipped, and degraded to mimic the resolution of the other input datasets. The mean horizontal accuracy of the NED was evaluated by the USGS using 13 305 geodetic control points nationwide and was found to be 2.44 m. The mean vertical accuracy was found to be 1.64 m based on 9187 unique pairs of geodetic reference points (USGS, 2011). The NED data was the coarsest resolution utilized in this research. Because of the requirements of the decision-tree algorithm used in this research, all other datasets were resampled to the same 10 m spatial resolution.

Slope and curvature were generated from the NED by running tools in the Environmental Systems Research Institute (ESRI) ArcGIS software. The assumption behind using these derived products from elevation data was that they contained additional information that describes physical characteristics about the drainage of water in a basin, where the slope of a landscape can affect the rate of flow of water and the curvature influences the convergence and divergence of that flow (Moore et al., 1991).

Radar

Two fully polarimetric C-band (5.6 cm wavelength) RADARSAT-2 look complex SAR images were obtained through the Canadian Space Agency's Science and Operational Applications Research (SOAR) Program. The dates of these images were 15 June and 19 September 2009. Fully polarimetric SAR imagery is collected with varying transmitted and received signal polarizations (horizontal–horizontal, HH; vertical–vertical, VV; horizontal–vertical, HV; and vertical–horizontal, VH). In addition, two dates of polarimetric decomposition products were obtained through the Canada Center for Remote Sensing for 9 July and 26 August 2009. All SAR images for this research were acquired in fine quad-beam mode with near and far incidence angles of 26.9 and 28.7, respectively (FQ8). The constant beta look-up table was applied for calibration to avoid over saturation of the data (Kaya, 2010). A 7 × 7 boxcar filter was applied to each image to reduce speckle noise and increase the number of looks needed for polarimetric decomposition (**Figure 6**), and the images were resampled to 10 m spatial resolution. The digital number (DN) values, representing amplitude, were converted to sigma naught (σ^0) or backscattering coefficient in units of decibels for quantitative analysis (Parmuchi et al., 2002).

Response signatures of the SAR backscatter values for each polarization of two different periods in time for upland and wetland classified reference field sites are shown in **Figure 7**. As previously described for the optical response signatures, **Figure 8** shows how each wetland class is represented in the SAR response signature of wetlands as a whole. There are only slight differences between the backscatter response values of each wetland type for the two periods of the season. For example, there was no change in the peak HH response of emergent wetlands; however, the range of backscatter values in September shifted down by 5 decibels compared with June, possibly indicating a change in physical characteristics of the vegetation present later in the season. The HV response had a similar shift in the range of backscatter response values, but the peak response was 5 decibels lower for emergent wetlands in September. Looking at the response signatures of scrub/shrub wetlands, there was no discernible difference between June and September backscatter values in each of the polarizations in terms of the peak backscatter or range of values. The range of HH backscatter values for forested wetlands was the same for June and September; however, the peak values similarly shifted 5 decibels lower in September compared with June. The VV response for forested wetlands had a 5 decibel shift downward in the range of backscatter values from June to September. Though these shifts in peak backscatter value

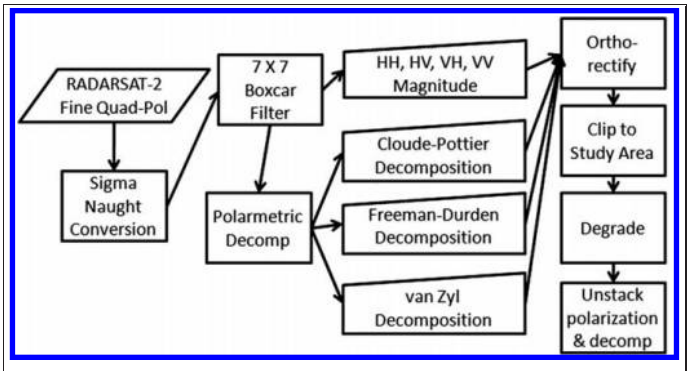

Figure 6. Synthetic aperture radar (SAR) input data, preprocessing methods, and output data for decision-tree classification.

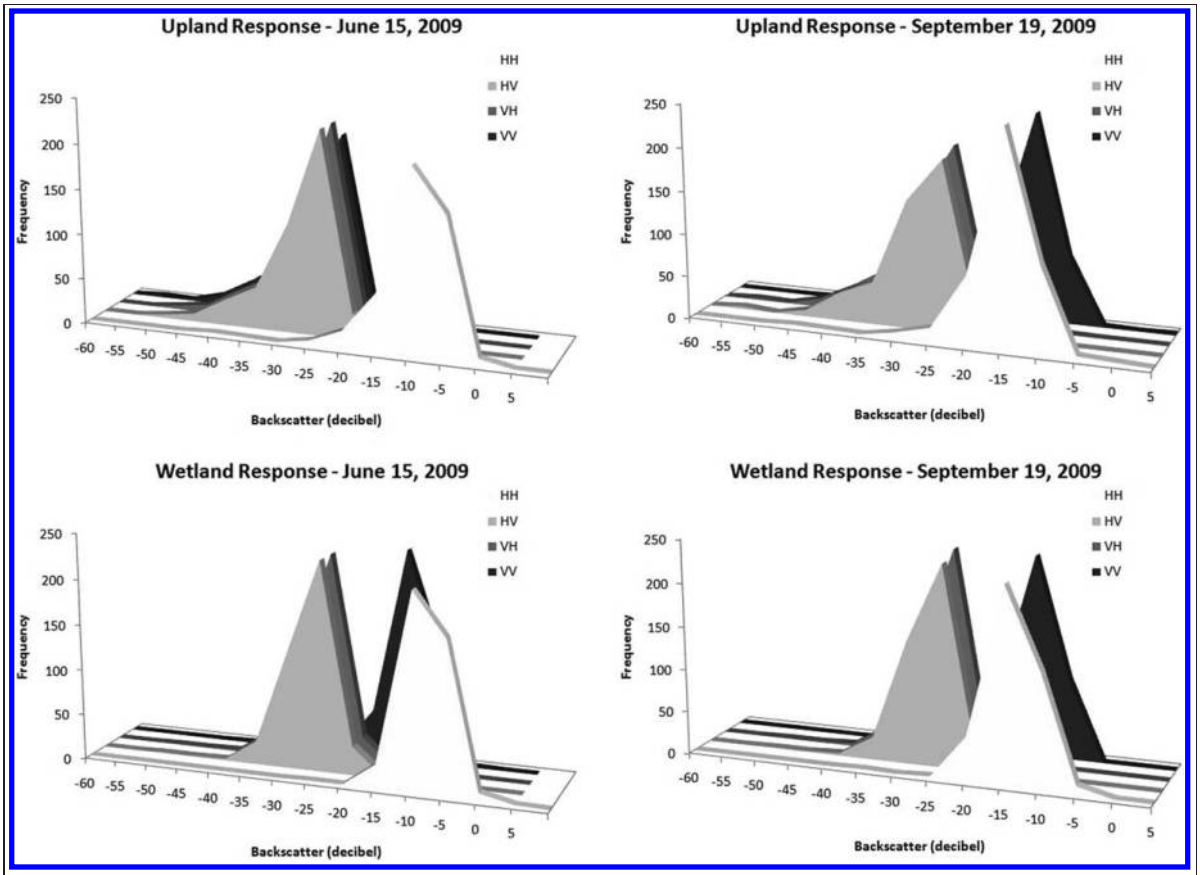

Figure 7. Spectral response signatures for each of the SAR polarizations extracted from field reference data points of upland and wetland class categories and for each SAR image date: 15 June 2009 and 19 September 2009.

and the range and variability of backscatter values per image date, land class type, and polarization were subtle, the decision-tree classification method was expected to use this information to improve the results of the wetland classification.

Polarimetric decompositions were used to assess the importance of radar polarimetry on the accuracy of wetland mapping. Combinations and differences between the transmitted and received signal polarizations detected vegetation differences quite well (Baghdadi et al., 2001; Henderson and Lewis, 2008; Slatton et al., 2008). Many supervised and unsupervised algorithms have been developed to exploit multiple polarization data to distinguish physical features on the ground in a radar scene. This research used three of the most frequently used unsupervised polarimetric decompositions in the literature, including the Van Zyl, Freeman–Durden, and Cloude–Pottier decompositions and their related parameters. Each of the polarimetric decompositions was performed prior to orthorectification in an attempt to reduce resampling error, particularly in thematic decompositions.

The van Zyl polarimetric decomposition is an unsupervised thematic classification based on the phase and backscatter response of scattering targets on the ground (van Zyl, 1989). Each pixel is categorized as a single, odd, or diffuse scatterer based on the number of phase shifts that occurred per pixel between co-polarized (HH and VV) scattering waves, where every scattering event is expected to add a 180° phase shift. The van Zyl decomposition product therefore is a single thematic layer per SAR image date.

The Freeman–Durden polarimetric decomposition is similar to van Zyl's in that it is a technique for identifying physically-based scattering mechanisms on the ground. However, the Freeman–Durden decomposition effectively breaks down the total backscatter for each pixel into relative portions of three scattering mechanisms: surface scatter, double bounce, and canopy scatter (or volume scatter). Each pixel then has a relative weight for each scattering mechanism, instead of a single category (Freeman and Durden, 1998). The Freeman–Durden decomposition product is therefore three layers of data per image date.

The third polarimetric decomposition utilized in this paper was presented by Cloude and Pottier (1997). In this decomposition, the parameters of entropy, alpha angle, and anisotropy are calculated from the eigenvalues and eigenvectors of the coherency matrix. Cloude and Pottier showed that these parameters represent different scattering mechanisms, directly relating to the affect that the physical structure of the target has on the received backscatter.

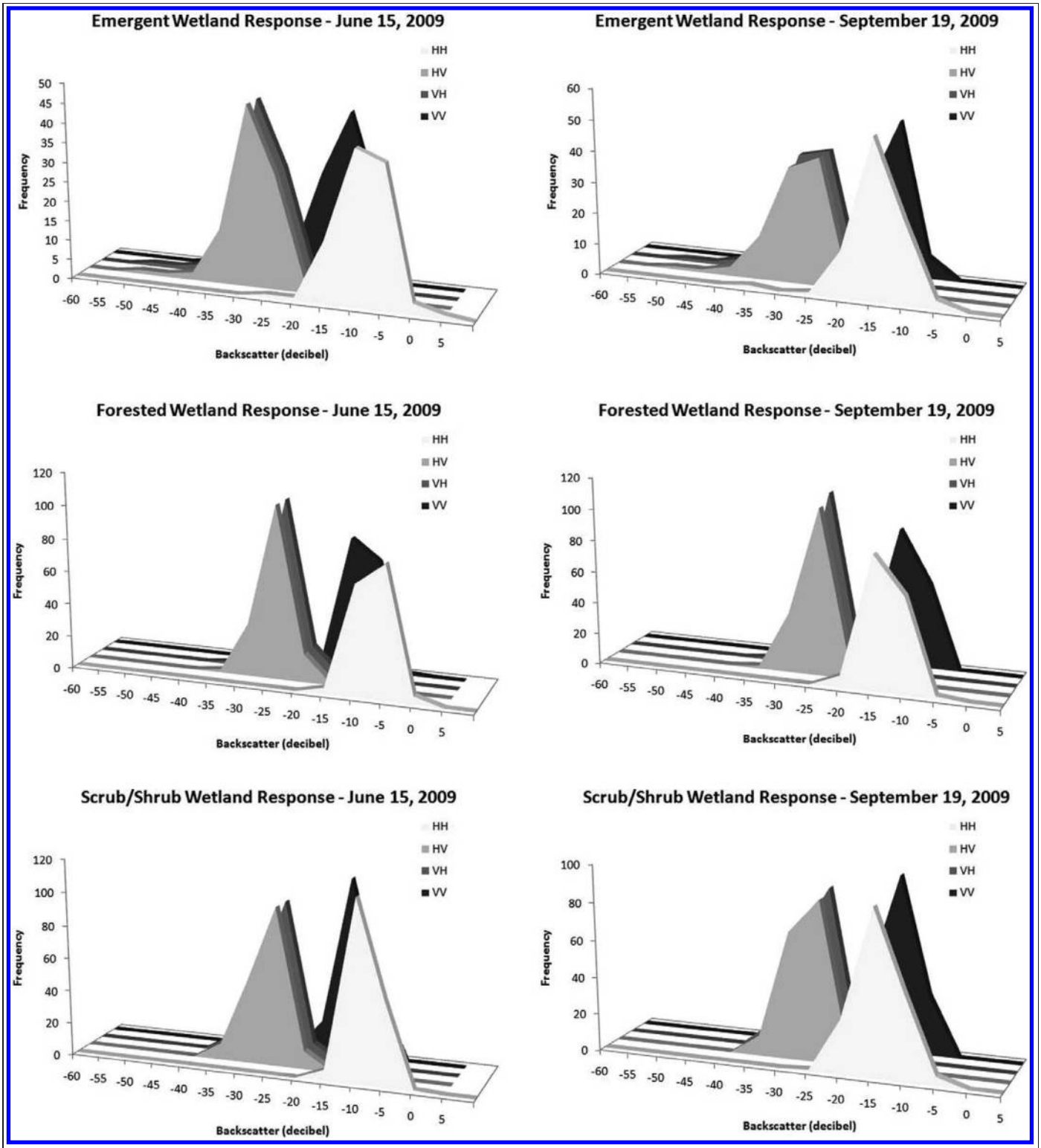

Figure 8. Spectral response signatures for each of the SAR polarizations extracted from field reference data points of emergent, forested, and scrub/shrub wetland class types and for each SAR image date: 15 June 2009 and 19 September 2009.

Entropy is defined as the randomness of scattering, alpha angle is indicative of the dominant scattering mechanism, and anisotropy is a parameter that indicates whether there are multiple scattering mechanisms occurring. Cloude and Pottier (1997) also developed an unsupervised classification scheme based on regions of the entropy, alpha, anisotropy space. This research utilizes the parameters entropy, alpha angle, and anisotropy as separate layers in the classifier, in

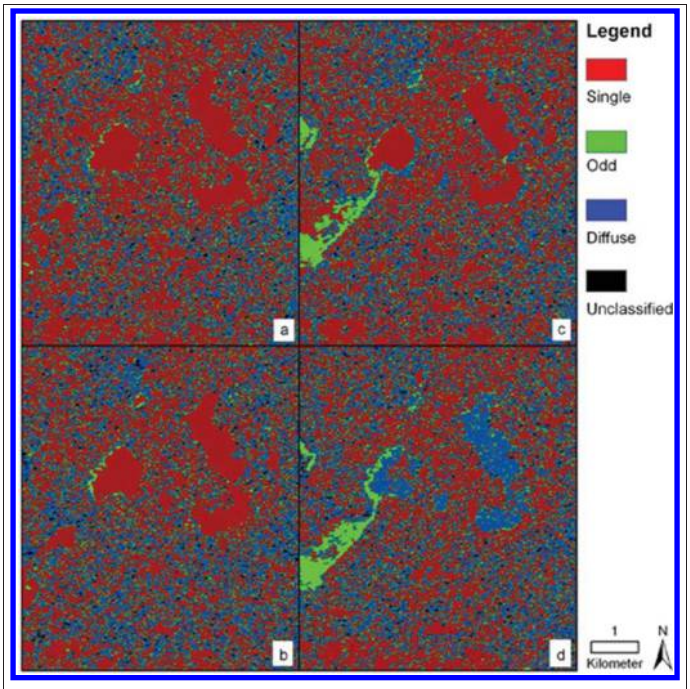

Figure 9. Subset area showing the van Zyl SAR polarimetric decomposition results for all four dates used in this research: (a) 15 June 2009, (b) 9 July 2009, (c) 26 August 2009, and (d) 19 September 2009.

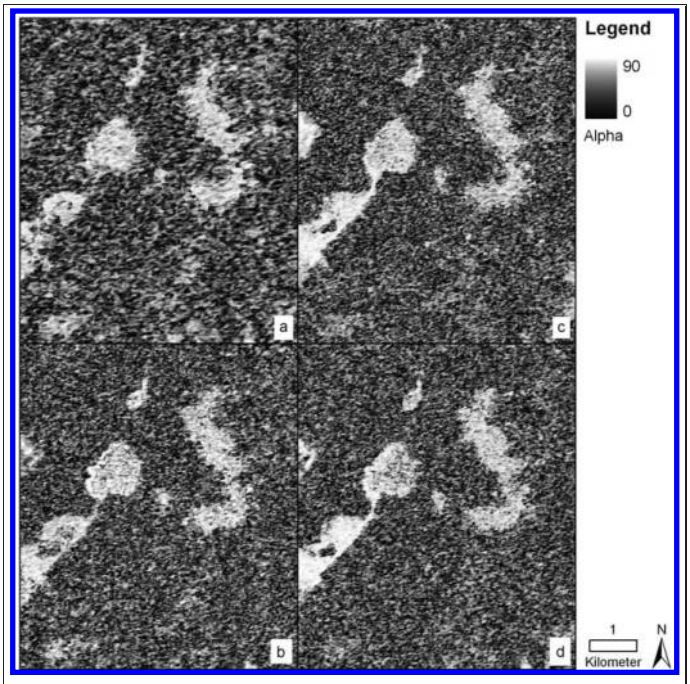

Figure 11. Subset area showing the Cloude–Pottier SAR polarimetric decomposition parameter alpha for all four dates used in this research: (a) 15 June 2009, (b) 9 July 2009, (c) 26 August 2009, and (d) 19 September 2009.

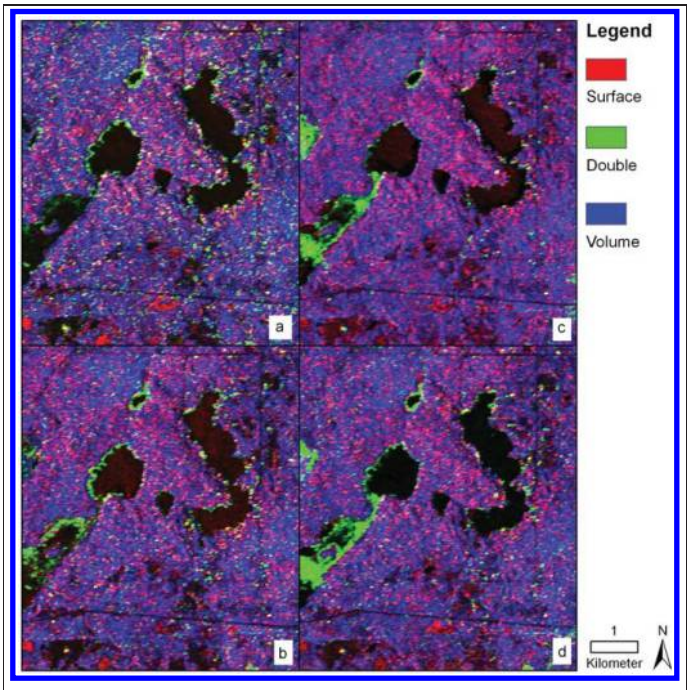

Figure 10. Subset area showing the Freeman–Durden SAR polarimetric decomposition results for all four dates used in this research: (a) 15 June 2009, (b) 9 July 2009, (c) 26 August 2009, and (d) 19 September 2009.

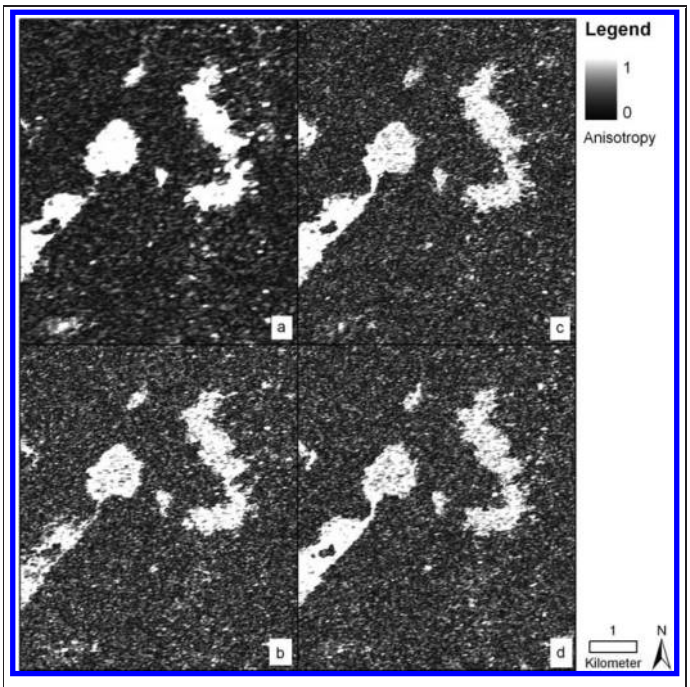

Figure 12. Subset area showing the Cloude–Pottier SAR polarimetric decomposition parameter anisotropy for all four dates used in this research: (a) 15 June 2009, (b) 9 July 2009, (c) 26 August 2009, and (d) 19 September 2009.

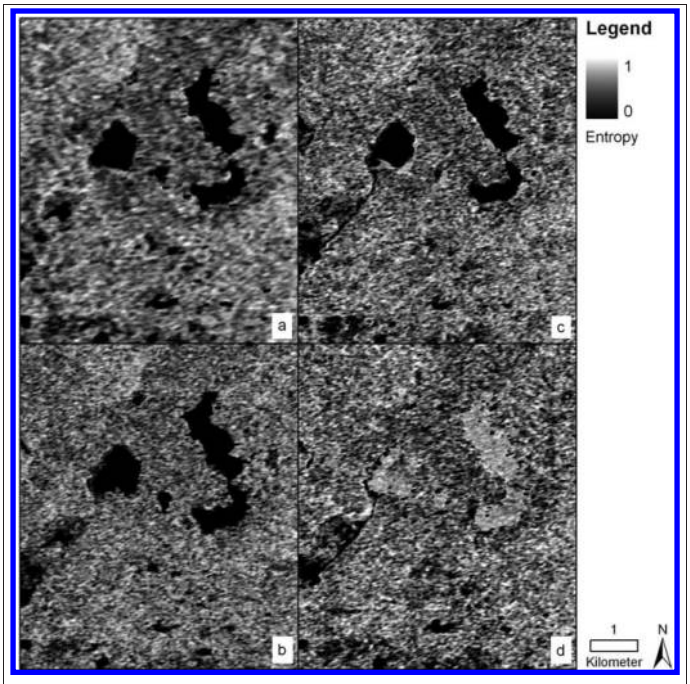

Figure 13. Subset area showing the Cloude–Pottier SAR polarimetric decomposition parameter entropy for all four dates used in this research: (a) 15 June 2009, (b) 9 July 2009, (c) 26 August 2009, and (d) 19 September 2009.

addition to the thematic Cloude–Pottier classification product, totalling four layers of data per image date.

To finish preparing SAR data for the decision-tree classifier, the polarimetric decompositions and associated data layers, plus the backscattering coefficient for each polarization, were stacked for each SAR image date. The stacked image dates were then co-registered using 30 evenly distributed tie points and orthorectified using the 2008 aerial orthophotos and NED (**Figure 3**). The boxcar filter, calculation of σ^0, polarimetric decomposition processing, and orthorectification of SAR images were completed using PCI Geomatica and the image clip and spatial resolution resampling procedures were done using ERDAS Imagine software.

Accuracy assessment

To assess the accuracy of the decision tree classification results, the aforementioned independent reference dataset was utilized (25% of the field point data). Error matrices were produced for both the upland/water/wetland determinant and modified Cowardin classifications, as well as both input dataset combinations of optical/topographic and optical/topographic/SAR input data. For each classification, user's and producer's accuracies were calculated, along with errors of omission and commission, overall accuracy, and the kappa statistic (k-hat) (Congalton and Green 1999). A significance test of both error matrix k-hat values was used to compare the input dataset combinations. In addition to the above analyses, the overall accuracy of the original NWI data was assessed using the same independent reference points. A similar k-hat significance test was performed between the optical/topographic/SAR input dataset and the NWI for each classification scheme.

A classification tree is created using training data to determine, branch-by-branch, the best dichotomous split to reduce intraclass variability and the resulting ruleset is applied to the whole set of input data. RandomForest has the capacity to grow multiple decision trees and the end result is a classification tree, which received the best vote of confidence by cross-validation. The outputs of the randomForest classification described in this paper include: (*i*) a

Table 2. Error matrices and associated accuracy results from the upland/water/wetland determinant classification using optical and topographical data only and for using optical, topographic, and SAR imagery combined.

	Reference data					
Classified data	Upland	Water	Wetland	Row total	User accuracy (%)	Commission error (%)
Optical and Topographical input data only						
Upland	121	2	43	166	73	27
Water	0	13	3	16	81	19
Wetland	30	8	94	132	71	29
Column total	151	23	140	315		
Producers accuracy (%)	80	57	67			
Omission error (%)	20	43	33			
Optical, Topographical, and SAR data						
Upland	119	6	35	160	74	26
Water	1	13	2	16	81	19
Wetland	32	4	103	139	74	26
Column total	152	23	140	315		
Producers accuracy (%)	78	57	74			
Omission error (%)	22	43	26			

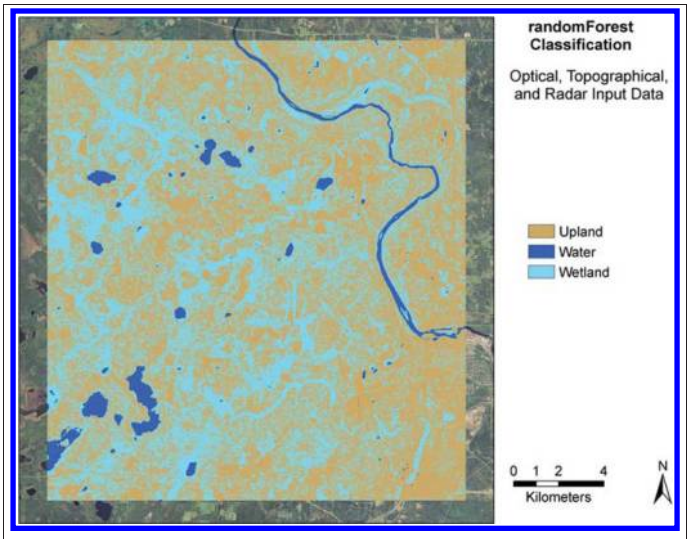

Figure 14. Upland/water/wetland determinant classification result from a randomForest decision-tree classification using a combination of optical, topographical, and SAR imagery as inputs data in the classifier.

measure of confidence per cell, created by cross-validating observed versus predicted classes; (*ii*) the gini index, which is used to evaluate the most significant input layers; and (*iii*) the mean decrease in accuracy per input layer.

The gini index corresponds to the structure of a decision tree, such that every time a split is determined by an input variable, there is a resulting decrease in the gini index for that variable (Breiman, 2001). The mean decrease in accuracy is determined by the resulting accuracy from several out-of-bag samples, in which a variable is randomly included or excluded and the resulting change in the overall accuracy for all trees is averaged (Breiman, 2001). The partial dependence of specific values of a variable is determined by comparing the error rate from an out-of-bag sample using a random selection of values to the error rate of the same out-of-bag sample using all values of that variable. The result is a graphical description, or profile, of the effect that a variable's values have on the class probability, after accounting for the effects of the other variables. The *y*-axis of a partial dependence plot is the predicted function and log of the fraction of votes (logits) for the classification (Breiman, 2001). In this study, the most important variables in the classification were determined by both the gini index and the mean decrease in accuracy. A selection of the top input variables were evaluated for the partial dependence of its values.

Results and discussion

Polarimetric decompositions

The results for the van Zyl polarimetric decomposition are shown in **Figure 9**. There were a few notable trends. For the frequency of pixels classified as odd and diffuse scattering increased, but surface scattering decreased over time. The increase of odd and diffuse scattering was particularly noticeable around the water bodies in the central part of the area of interest. Looking back at the spring and summer aerial orthophotos in **Figure 2**, there was a noticeable change of emergent vegetation around the water bodies between the summer and spring images. Single scattering decreased generally over time, but stayed the same in certain areas, notably the south part of **Figure 8** where there is urban development.

The Freeman–Durden polarimetric decomposition results are shown in **Figure 10**. Beyond the trend in increased double-bounce scattering around the water bodies, similar to the findings in the van Zyl decomposition, there was a trend toward a higher fraction of volume scattering per pixel over time (indicated by the increased frequency of bluer pixels). In **Figure 2**, the areas that have a concentration of volume scattering pixels appear to be forested wetlands and the areas in that have a concentration of mixed double/volume scattering pixels (indicated by the magenta color) tend to be upland forest.

The results from the Cloude–Pottier decomposition are shown in **Figures 11–13**. The parameter alpha, indicative of the dominant scattering mechanism, appears to be fairly noisy in all four dates (**Figure 11**). However, a closer look at the map reveals that there was a slight trend toward more definition of surface features, where the central water bodies were outlined by high alpha values. Overall, June had the lowest range and mean alpha angles and August had the highest, likely due to differences in maturation and density of vegetation in these two time periods.

The result of the Cloude–Pottier decomposition parameter anisotropy, indicative of the presence of multiple scattering mechanisms, or surface roughness, is shown in **Figure 12**. High anisotropy values indicated that the scattering was predominantly singular scattering mechanisms, while low values indicated multiple scattering types. The water bodies, as expected, had anisotropy values indicative of a specular scattering mechanism, however, it was difficult to discern differences in other land cover types.

The last Cloude–Pottier parameter examined was entropy, which indicated the relative randomness of scattering on the ground, as shown in **Figure 13**. Entropy and anisotropy had an inverse relationship, where areas that had multiple scattering mechanisms (low anisotropy values) had a high degree of randomness (high entropy values). Looking at the water bodies in the central part of the figure, it makes sense that the entropy values were low while the anisotropy values were high. However, later in September (**Figure 13b**), the entropy values increased in the same areas that saw an increase in the van Zyl diffuse scattering mechanisms. This was likely due to the wind causing small changes of the water surface and not likely indicative of a change in vegetation.

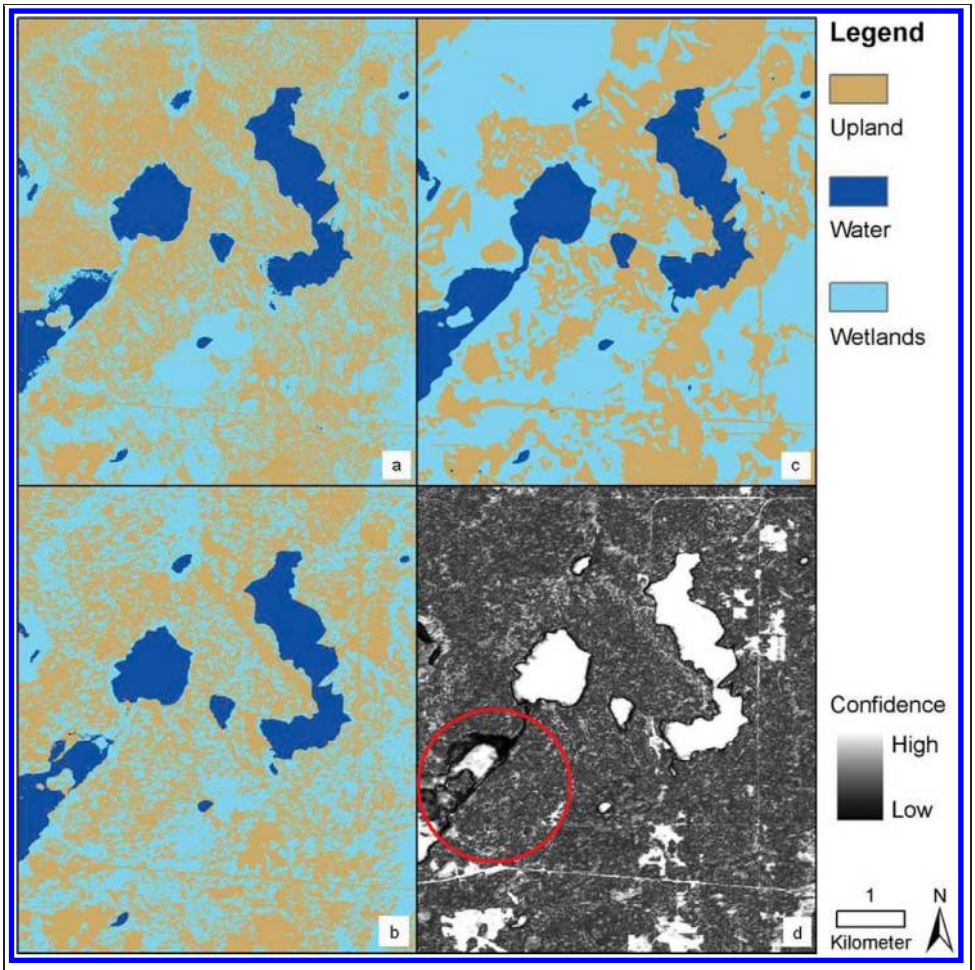

Figure 15. Subset area showing the upland/water/wetland determinant classification results from a randomForest decision-tree classification: (a) using optical and topographical data alone and (b) using optical, topographic, and SAR imagery combined. The original National Wetland Inventory (NWI) data is shown in panel (c), where land cover classes were consolidated for ease in comparison. The relative confidence of the decision tree classification using all optical, topographic, and radar data is shown in panel (d).

Upland/water/wetland determinant classification

The first classification analysis presented is the result from the upland/water/wetland determinant classification. The error matrix in **Table 2** illustrates that without the inclusion of SAR data, the decision-tree classifier confused upland areas with wetland areas 27% of the time (commission error) and by including all available SAR data there was a slight improvement to 26% commission error. The largest improvement in terms of differentiating between upland/water/wetland was in the omission error of wetlands, meaning SAR data helped to ensure that more reference points were correctly classified as wetlands. The output classification map for the entire study area can be seen in **Figure 14**.

A subset area was chosen to illustrate an area with diverse land cover and seasonality (**Figure 2**). **Figure 15** shows that differentiation between the upland/water/wetland classes was fairly similar between the two decision-tree tests (optical/topographical only versus optical/topographic/SAR included); however, both classifications were quite different from that of the original NWI. As it is based on older imagery, the NWI may not reflect land use change of wetlands being converted to other upland classes. As a result, the NWI appeared to significantly overestimate wetland area compared with this classification based on current imagery. It is also important to point out areas with relatively low confidence in the classification result. For example, the confidence of the shoreline of a southwest lake (circled in **Figure 15d**) was particularly low. This was likely due to the apparent seasonality observed in the aerial photos of **Figure 2** and a possible lack of temporal coverage to accommodate the seasonality.

The mean decrease in accuracy and gini index plots from randomForest were assessed in **Figure 16**, which shows the most effective input datasets for the upland/water/

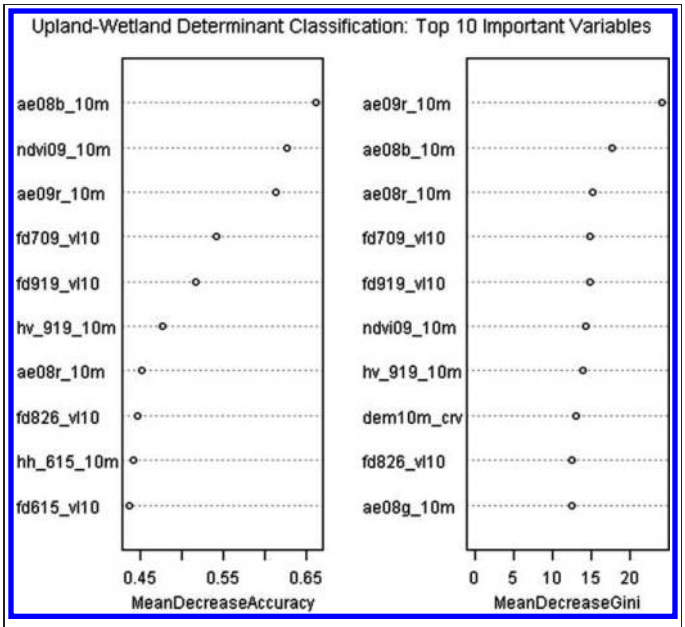

Figure 16. Mean decrease accuracy and gini index plots for the upland/water/wetland determinant classification using optical, topographic, and SAR imagery combined.

wetland determinant classification. Among these, the most important input variables include: the blue and red bands of 2008 leaf-on aerial orthophoto (“ae08b_10m” and “ae08r_10m”), the red band and NDVI of 2009 early leaf-onset aerial orthophoto (“ae09r_10m” and “ndvi09_10m”),

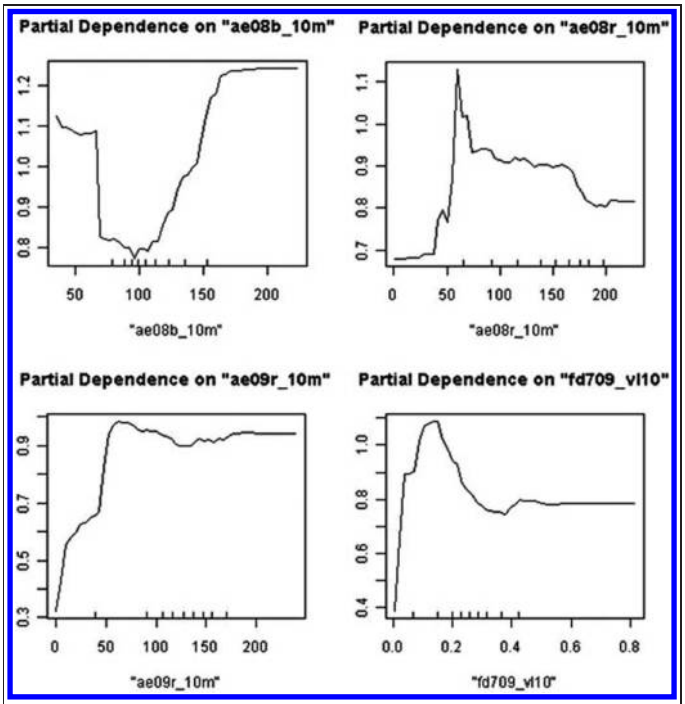

Figure 17. Value partial dependence plots for a selection of the most important input variables for the upland/water/wetland determinant classification using optical, topographic, and SAR imagery combined.

and the Freeman–Durden volume scattering parameter from the mid-summer 7 July 2009 image (“fd709_vl10”). It was interesting to note the relative values for each dataset that were most sensitive to the accuracy of the classification (**Figure 17**). These partial dependence plots indicated the values with higher probability of significance for improving the accuracy of the classification. For example, the DN values of the red band that are responsible for improving the classification accuracy (around 45–65) were similar for both the early leaf-onset and leaf-on mid-summer aerial photos. Conversely, the DN values less than 75 or greater than 150 of the blue band in the leaf-on aerial photo were the most probable in improving the accuracy of the classification.

Though SAR input data were not among the most important variables for decision-tree classification, several layers were in the top ten, including: the volume scattering channel of the Freeman–Durden polarimetric decomposition from all four image dates utilized in this study, the HH channel from 15 June 2009, and the HV channel from 19 September 2009. These results illustrated that including relative backscatter as well as polarimetric information about scattering mechanisms typically observed by vegetative canopies helped improve upland/water/wetland classification accuracy. Although the Freeman–Durden parameters were important in the accuracy of the classification, it was difficult to assess the partial dependence of specific values of one scattering mechanism without knowing the relative percentage of the other two scattering mechanisms. The least important input datasets were found to be the thematic polarimetric decompositions of Cloude–Pottier and, most particularly, van Zyl. These findings were likely due to the limiting and unrealistic nature of assigning a single scattering mechanism to each pixel on the ground.

Modified Cowardin land cover classification

Table 3 shows the error matrix for the modified Cowardin classification. With optical and topographic data alone, the decision-tree classifier confused scrub/shrub areas 51% of the time (commission error) and mainly misclassified these areas as upland. Unfortunately, there was no improvement in commission error of scrub/shrub wetlands by including SAR data, mainly due to the additional confusion with forested wetlands. The addition of SAR improved the accuracy of classifying water but there was little difference in the omission or commission errors of the upland and wetland classes. The output of this classification for the entire study area is shown in **Figure 18**.

In the same subset area as discussed previously, **Figure 19** shows how the modified Cowardin classification results are again visually similar between the two decision-tree tests (optical/topographical only versus optical/topographic/SAR included), but vary greatly from that of the original NWI. It was clear that the original NWI estimated a much higher coverage of forested wetlands and little scrub/shrub in comparison. Pointing out the same

Table 3. Error matrices and associated accuracy results from the modified Cowardin land cover classification using optical and topographical data only and for using optical, topographic, and SAR imagery combined.

	Reference data							
Classified data	Water	Emergent wetlands	Forested wetlands	Scrub/shrub wetlands	Upland	Row total	User accuracy (%)	Commission error (%)
Optical and topographical input data only								
Water	13	3	0	0	1	17	76	24
Emergent wetlands	6	15	2	3	3	29	52	48
Forested wetlands	0	0	17	8	8	33	52	48
Scrub/shrub Wetlands	0	6	6	31	20	63	49	51
Upland	4	13	23	13	120	173	69	31
Column Total	23	37	48	55	152	315		
Producers accuracy (%)	57	41	35	56	79			
Omission error (%)	43	59	65	44	21			
Optical, Topographical, and SAR Data Included								
Water	16	2	0	0	1	19	84	16
Emergent wetlands	3	15	1	3	5	27	56	44
Forested wetlands	0	0	19	10	12	41	46	53
Scrub/shrub wetlands	1	11	9	31	15	67	46	54
Upland	3	9	19	11	119	161	74	26
Column total	23	37	48	55	152	315		
Producers accuracy (%)	70	41	40	56	78			
Omission error (%)	30	59	60	44	22			

southwestern lake as described previously, the confidence in classification of wetland type increased (**Figure 19d**) and there were few areas within this subset area that had very low confidence.

The mean decrease in accuracy and gini index plots from randomForest for the modified Cowardin classification are shown in **Figure 20**. The most important input datasets for this classification include: the blue and red bands of the 2008

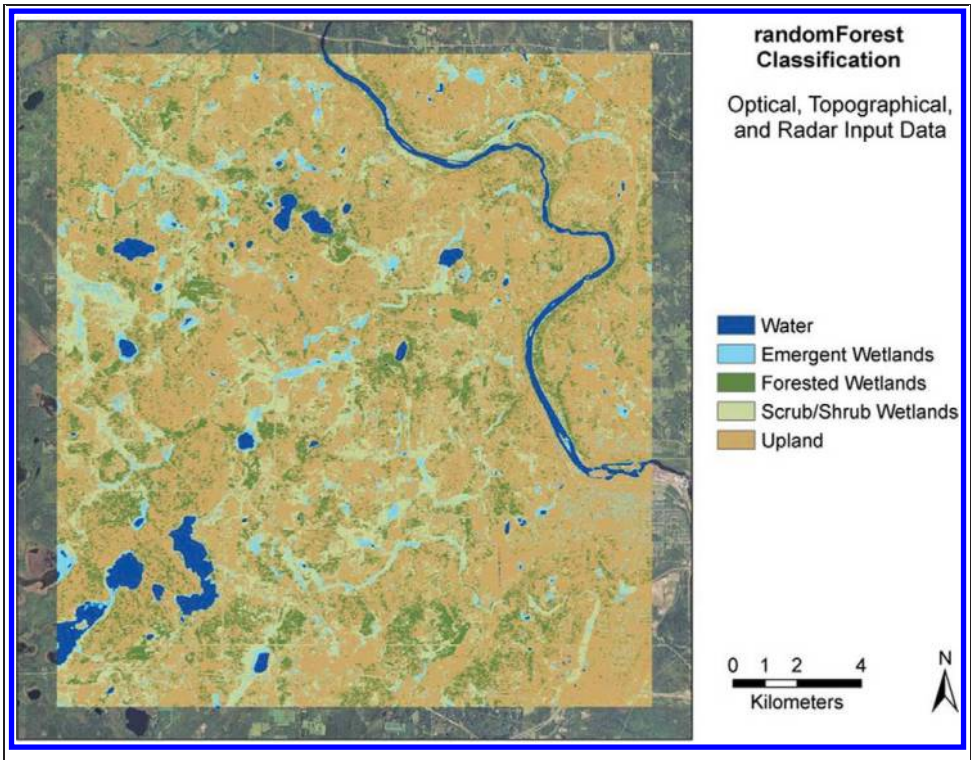

Figure 18. A modified Cowardin land cover classification result from a randomForest decision tree classification using a combination of optical, topographical, and SAR imagery as inputs data in the classifier.

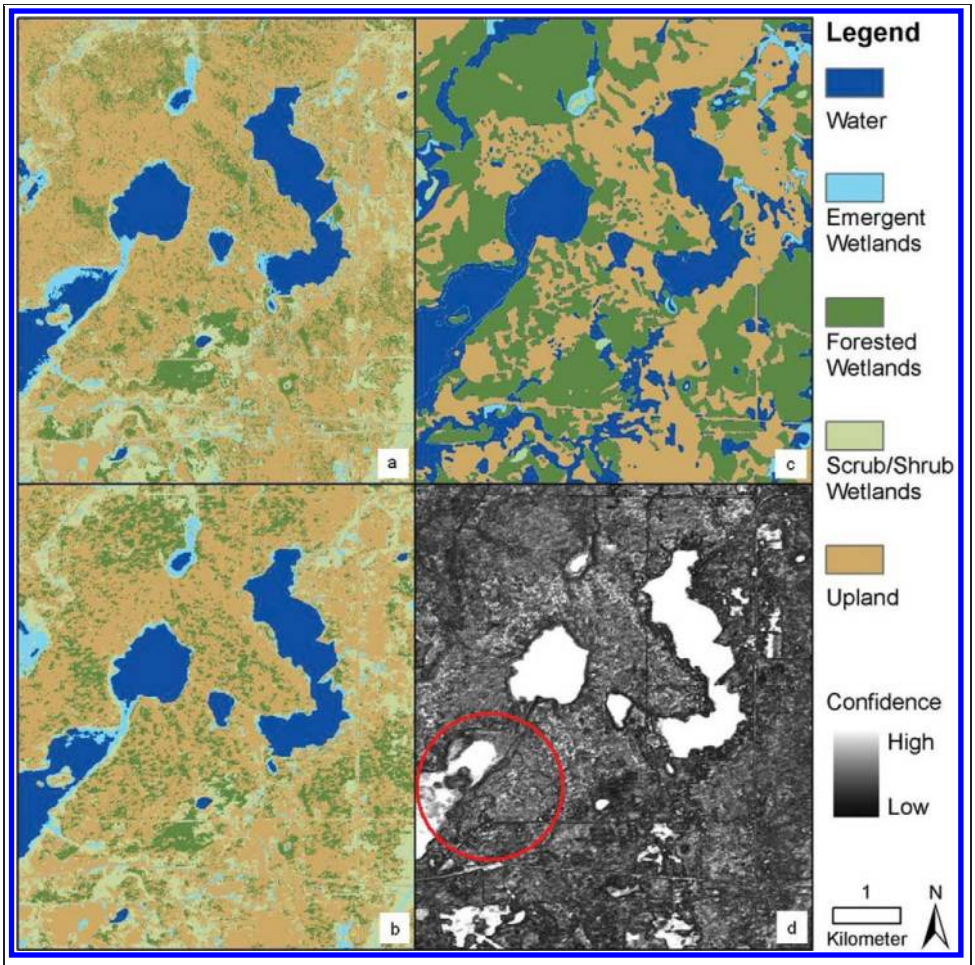

Figure 19. Subset area showing the upland/water/wetland determinant classification results from a randomForest decision tree classification: (a) using optical and topographical data alone and (b) using optical, topographic, and radar imagery combined. The original National Wetland Inventory (NWI) data is shown in panel (c), where land cover classes were consolidated for ease in comparison. The relative confidence of the decision tree classification using all optical, topographic, and radar data is shown in panel (d).

leaf-on aerial orthophoto ("ae08b_10m" and "ae08r_10m"), the red band and NDVI of 2009 early leaf-onset aerial orthophoto ("ae09r_10m" and "ndvi09_10m"), and elevation ("dem_10m"). Except for the apparent dependence on elevation, the important variables for the modified Cowardin classification were not very different from the variables important for upland/water/wetland determinant classification. However, it was most interesting that the sensitive DN values for each of these datasets were very different (**Figure 21**). Here, DN values of the leaf-on blue band that were least important for the upland/water/wetland determinant classification were among the most important values for the Cowardin classification. A similar pattern was found with the important values in the early leaf-onset red band, where the DN values below 45 were much more important in the Cowardin classification than for the upland/water/wetland determinant classification. These findings strengthened the case for the inclusion of seasonal aerial orthophotos for improving wetland mapping accuracy.

Similar to the previous findings, the volume scattering channel of the Freeman–Durden polarimetric decomposition from most image dates and the HV channel from June were found to be important for classifying wetland types. Again, these results illustrated that including relative backscatter as well as polarimetric information can improve wetland mapping accuracy over having the broad thematic definitions of surface scattering mechanisms.

Table 4 shows a comparison of all error matrices for each classification scheme. The addition of SAR data in the upland/water/wetland determinant classification improved the accuracy by 3% over having optical and topographical data alone and by 5% over the original NWI. Each of the upland/water/wetland classification error matrices were found to have statistically significant z statistics, but the differences between the optical/topographic and optical/

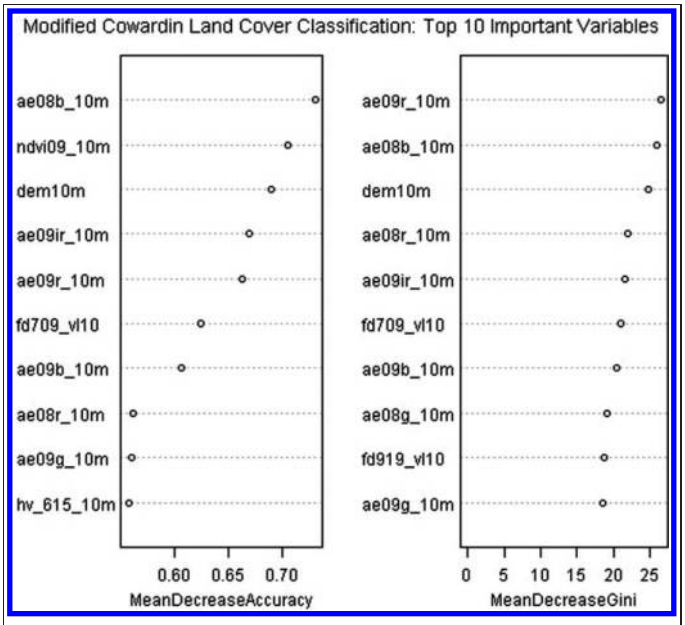

Figure 20. Mean decrease accuracy and gini index plots for the modified Cowardin land cover classification using optical, topographic, and SAR imagery combined.

topographic/SAR matrices and between the optical/topographic/SAR and NWI matrices were not statistically significant. For the modified Cowardin classification scheme, the addition of SAR data only improved the accuracy 1% over having optical and topographical data alone. However, a comparison of the *z* statistics from the original NWI and optical/topographic/SAR matrices showed that this method significantly improved the classification wetland types, increasing the accuracy by 14%.

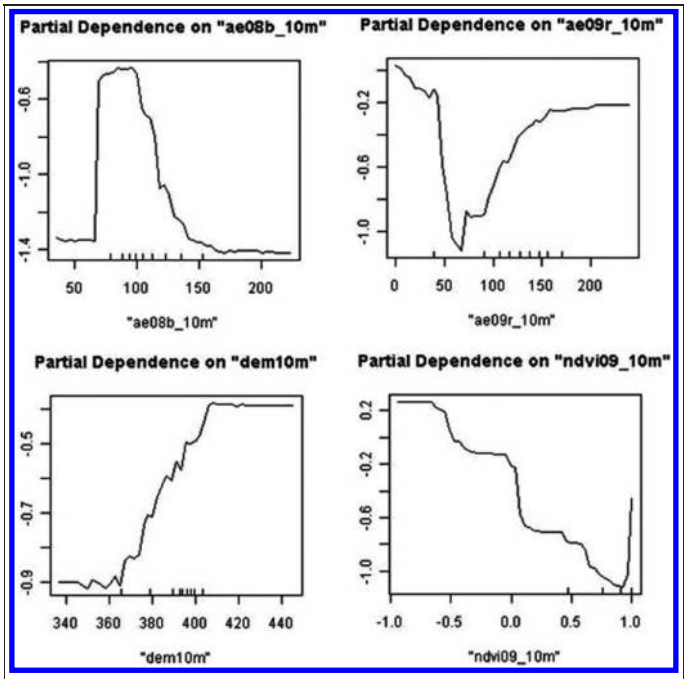

Figure 21. Value partial dependence plots for a selection of the most important input variables for the modified Cowardin land cover classification using optical, topographic, and SAR imagery combined.

Summary and conclusion

The research presented here showed that the integration of multitemporal, multisensor, and multifrequency remotely sensed data improved the accuracy of a decision-tree classification of wetlands in a forested region of northern Minnesota. Forested wetlands are typically very challenging to map, due to the obstruction of tree canopy cover. The incorporation of radar backscatter and polarimetric data was shown to improve the commission error of forested wetlands and improved the overall accuracy of all wetland types. The original NWI has many disadvantages and this study offered a method to improve the classification accuracy of wetlands using a robust, free, decision-tree algorithm.

The potential to apply the methodology presented in this paper over another study site is limited mainly by input imagery and training data availability. Currently, SAR data is not freely available and can be expensive if fully polarimetric imagery is desired over large geographic areas. However, certain landscapes may not benefit from the addition of SAR data, particularly if there is very little tree canopy or if the weather is always clear.

The prevailing advantage of longer wavelength radar signals is thought to be their circumvention and deeper penetration of dense canopy cover. Though SAR data improved the accuracy of differentiating between upland and wetland areas, the performance of the decision-tree classifier was not significantly different than without SAR for this study site. Changes in surface structure directly affected backscatter brightness and classified scattering mechanisms. However, the temporal variability in these land classes are apparently not significant enough that SAR data contributed considerable improvement to the accuracy of the land cover classifications shown in this paper. Further research is therefore needed in other SAR sensor platforms with longer wavelengths, such as the Advanced Land Observing Satellite Phased Array type L-band Synthetic Aperture Radar (23 cm wavelength) data and in alternative optical platforms with more spectral bands available, such as the Landsat Thematic Mapper. Incorporation of optical, topographic, C-band, and L-band data may increase the accuracy of classifying forested wetlands.

The results of this study included a wetland classification map and the relative confidence of each pixel. The methods presented here provide a valuable tool for automated mapping of wetland areas and provide an effective aid for facilitating the manual mapping of more challenging wetland class types using aerial photos and a human interpreter.

Table 4. Summary of the independent accuracy assessment results from both decision-tree classification schemes (upland/water/wetland determinant and modified Cowardin class) and for both input dataset combinations of optical/topographic input data only and optical/topographic/SAR input data. Using the same independent reference data points, an accuracy assessment was also done on the original National Wetland Inventory (NWI).

Land cover classification	Total accuracy	Kappa-hat statistic	Kappa-hat variance	Z statistic (significant)	Compare Z statistic
Upland–wetland determinant					
Optical and topographical input data only	72	0.51	0.0021	11.1*	0.6
Optical, topographical, and SAR data included	75	0.54	0.0020	12.2*	
Original National Wetland Inventory (NWI)	70	0.47	0.0021	10.3*	1.1
Modified Cowardin class					
Optical and topographical input data only	62	0.44	0.0015	11.1*	0.53
Optical, topographical, and SAR data included	63	0.47	0.0015	12.2*	
Original National Wetland Inventory (NWI)	49	0.31	0.0010	9.70*	3.2*

Acknowledgements

This research was carried out as part of a Canadian Space Agency's Science and Operational Applications Research (SOAR) Program project and was supported by the Minnesota Environment and Natural Resources Trust Fund and the Minnesota Department of Natural Resources. Special thanks are due to Brian Huberty of the U.S. Fish and Wildlife Service and Steve Kloiber of the Minnesota Department of Natural Resources, who initiated collaboration with the Canada Centre for Remote Sensing and secured project funding. The authors gratefully acknowledge the helpful comments of this paper's two reviewers.

References

Acharya, G., and Barbier, E. 2000. Valuing groundwater recharge through agricultural production in the hadejia-nguru wetlands in northern Nigeria. *Agricultural Economics*, Vol. 22, No. 3, pp. 247–259. doi: 10.1111/j.1574-0862.2000.tb00073.x.

Baghdadi, N., Bernier, M., Gauthier, R., and Neeson, I. 2001. Evaluation of C-band SAR data for wetlands mapping. *International Journal of Remote Sensing*, Vol. 22, No. 1, pp. 71–88. doi: 10.1080/01431160 1750038857.

Ban, Y., Hu, H., and Rangel, I. 2010. Fusion of Quickbird MS and RADARSAT SAR data for urban land-cover mapping: Object-based and knowledge-based approach. *International Journal of Remote Sensing*, Vol. 31, No. 6, pp. 1391–1410. doi: 10.1080/0143116090 3475415.

Breiman, L. 2001. Random forests. *Machine Learning*, Vol. 45, No. 1, pp. 5–32. doi: 10.1023/A:1010933404324.

Brisco B., Touzi R., van der Sanden, J., Charbonneau, F., Pultz, T., and D'Iorio, M. 2008. Water resource applications with RADARSAT-2: A preview. *International Journal of Digital Earth*, Vol. 1, No. 1, pp. 130–147. doi: 10.1080/17538940701782577.

Brooks, R., Wardrop, D., and Cole, C. 2006. Inventorying and monitoring wetland condition and restoration potential on a watershed basis with examples from Spring Creek Watershed, Pennsylvania, USA. *Environmental Management*, Vol. 38, pp. 673–687. doi: 10.1007/s00267-004-0389-y.

Bwangoy, J., Hansen, M., Roy, D., Grandi, G., and Justice, C. 2010. Wetland mapping in the Congo basin using optical and radar remotely sensed data and derived topographical indices. *Remote Sensing of Environment*, Vol. 114, No. 1, pp. 73–86. doi: 10.1016/j.rse.2009.08.004.

Campbell, J. 2007. *Introduction to Remote Sensing.* Guilford Press, New York, p. 466.

Castañeda, C., and Ducrot, D. 2009. Land cover mapping of wetland areas in an agricultural landscape using SAR and Landsat imagery. *Journal of Environmental Management*, Vol. 90, No. 7, pp. 2270–2277. doi: 10.1016/j.jenvman.2007.06.030.

Cloude, S., and Pottier, E. 1997. An entropy based classification scheme for land applications of polarimetric SAR. *IEEE Transactions on Geoscience and Remote Sensing*, Vol. 35, No. 1, pp. 68–78. doi: 10.1109/36.551935.

Congalton, R., and Green, K. 1999. *Assessing the accuracy of remotely sensed data: principles and practices.* Lewis Publishers, Boca Raton, FL.

Cowardin L., Carter, F., and LaRoe, E. 1979. *Classification of wetlands and deepwater habitats of the United States.* U.S. Department of the Interior, Fish and Wildlife Service, Northern Prairie Publication, Jamestown, ND. Report No. 0421.

Dahl, T. 1990. *Wetlands losses in the United States 1780's to 1980's.* U.S. Department of the Interior, Fish and Wildlife Service, Office of Biological Services, Washington D.C.

Deschamps, A., Greenlee, D., Pultz, T., and Saper, R. 2002. Geospatial data integration for applications in flood prediction and management in the Red River Basin. *IEEE International, Geoscience and Remote Sensing*, Vol. 6, pp. 3338–3340.

Frappart, F., Seyler, F., Martinez, J., León, J., and Cazenave, A. 2005. Floodplain water storage in the Negro River Basin estimated from microwave remote sensing of inundation area and water levels. *Remote Sensing of Environment*, Vol. 99, No. 4, pp. 387–399. doi: 10.1016/j.rse.2005.08.016.

Freeman, A., and Durden, S. 1998. A three-component scattering model for polarimetric SAR data. *IEEE Transactions on Geoscience and Remote Sensing*, Vol. 36, No. 3, pp. 963–973. doi: 10.1109/36.673687.

Hearne, R. 2007. Evolving water management institutions in the Red River Basin. *Environmental Management*, Vol. 40, No. 6, 842 p. doi: 10.1007/s00267-007-9026-x.

Henderson, F., and Lewis, A. 2008. Radar detection of wetland ecosystems: A review. *International Journal of Remote Sensing,* Vol. 29, No. 20, pp. 5809–5835. doi: 10.1080/01431160801958405.

Hess, L., Melack, J., Novo, E., Barbosa, C., and Gastil, M. 2003. Dual-season mapping of wetland inundation and vegetation for the central Amazon Basin. *Remote Sensing of Environment*, Vol. 87, No. 4, pp. 404–428. doi: 10.1016/j.rse.2003.04.001.

Hogg, A., and Todd, K. 2007. Automated discrimination of upland and wetland using terrain derivatives. *Canadian Journal of Remote Sensing,* Vol. 33, pp. S68–S83. doi: 10.5589/m07-049.

Kaya, S. 2010. Personal communication, June 30, Ottawa, ON. Environment Canada, Canada Center for Remote Sensing.

Lu, Z., and Kwoun, O. 2008. RADARSAT-1 and ERS InSAR analysis over southeastern coastal Louisiana: Implications for mapping water-level changes beneath swamp forests. *IEEE Transactions on Geoscience and Remote Sensing*, Vol. 46, No. 8, pp. 2167–2184. doi: 10.1109/TGRS.2008.917271.

Minnesota Department of Administration (AdminMN), Office of Geographic and Demographic Analysis State Demographic Center. 2011. 2010 Census: Minnesota City Profiles. Available from http://www.demography.state.mn.us/CityProfiles2010/index.html [Accessed 22 November 2011].

Minnesota Department of Natural Resources (MN DNR). 2010 Wetlands Status and Trends. Available from http://www.dnr.state.mn.us/eco/wetlands/wstm_prog.html [Accessed 20 August 2010].

Minnesota Department of Natural Resources (MN DNR). Natural History – Minnesota's Geology. Available from http://www.dnr.state.mn.us/snas/naturalhistory.html [Accessed 31 March 2011].

Minnesota Geospatial Information Office (MnGeo), Geographic Data Clearinghouse. Minnesota Aerial Photography: 2008. Available from http://www.mngeo.state.mn.us/chouse/airphoto/program_details.html [Accessed 31 March 2011].

Minnesota Geospatial Information Office (MnGeo), Geographic Data Clearinghouse. Spring Aerial Imagery Program for Minnesota: 2009-2015. Available from http://www.mngeo.state.mn.us/chouse/airphoto/spring2009-2015.html [Accessed 31 March 2011].

Mitsch, W., and Gosselink, J. 2000. The value of wetlands: Importance of scale and landscape setting. *Ecological Economics*, Vol. 35, No. 1, pp. 25–33. doi: 10.1016/S0921-8009(00)00165-8.

Moore, I., Grayson, R., and Landson, A. 1991. Digital terrain modeling: A review of hydrological, geomorphological, and biological applications. *Hydrological Processes*, Vol. 5, pp. 3–30. doi: 10.1002/hyp.3360050103.

Ozesmi, S., and Bauer, M. 2002. Satellite remote sensing of wetlands. *Wetlands Ecology and Management*, Vol. 10, No. 5, pp. 381–402. doi: 10.1023/A:1020908432489.

Parmuchi, M., Karszenbaum, H., and Kandus, P. 2002. Mapping wetlands using multi-temporal RADARSAT-1 data and a decision-based classifier. *Canadian Journal of Remote Sensing*, Vol. 28, No. 2, pp. 175–186. doi: 10.5589/m02-014.

Ramsey, E. 1995. Monitoring flooding in coastal wetlands by using radar imagery and ground-based measurements. *International Journal of Remote Sensing*, Vol. 16, No. 13, 2495 p. doi: 10.1080/01431169508954571.

Ramsey, E., Rangoonwala, A., Middleton, B., and Lu, Z. 2009. Satellite optical and radar data used to track wetland forest impact and short-term recovery from Hurricane Katrina. *Wetlands*, Vol. 29, No. 1, pp. 66–79. doi: 10.1672/08-103.1.

Ruefenacht, B., Liknes, G., Lister, A., Fisk, H., and Wendt, D. 2008. Evaluation of Open Source Data Mining Software Packages. In *Forest Inventory and Analysis (FIA) Symposium 2008*, October 21–23, 2008, Park City, UT, USA. Edited by McWilliams, W. U.S. Department of Agriculture, Forest Service, Rocky Mountain Research Station, Fort Collins, CO. Addendum.

Slatton K.C., Crawford M.M., and Chang L.D., 2008. Modeling temporal variations in multipolarized radar scattering from intertidal coastal wetlands. *ISPRS Journal of Photogrammetry and Remote Sensing*. Vol. 63, pp. 559–577. doi: 10.1016/j.isprsjprs.2008.07.003.

Touzi, R. 2006. Wetland characterization using polarimetric RADARSAT-2 capability. 2006. In *IEEE international Conference on Geoscience and Remote Sensing Symposium*, July 31-August 4, 2006, Denver, CO, U.S.A. 1639 p.

Touzi, R., Deschamps, A., and Rother, G. 2009. Phase of target scattering for wetland characterization using polarimetric C-band SAR. *IEEE Transactions on Geoscience and Remote Sensing*, Vol. 47, No. 9, pp. 3241–3261. doi: 10.1109/TGRS.2009.2018626.

Townsend, P. 2001. Mapping seasonal flooding in forested wetlands using multi-temporal radarsat SAR. *Photogrammetric Engineering & Remote Sensing*, Vol. 67, No. 7, pp. 857–864.

Töyrä, J., Pietroniro, A., Martz, L., and Prowse, T. 2002. A multi-sensor approach to wetland flood monitoring. *Hydrological Processes*, Vol. 16, No. 8, pp. 1569–1581. doi: 10.1002/hyp.1021.

United States Department of Agriculture (USDA) Geospatial Data Gateway. Available from http://datagateway.nrcs.usda.gov/ [Accessed 31 March 2011].

United States Department of Agriculture (USDA) National Agricultural Statistics Service (NASS). Cropland Data Layer. Available from http://www.nass.usda.gov/research/Cropland/SARS1a.htm [Accessed 31 March 2011].

United States Fish and Wildlife Service. National wetlands inventory (NWI). Available from http://www.fws.gov/wetlands/ [Accessed 12 October 2009].

United States Geological Survey. Accuracy of the National Elevation Dataset (NED). Available from http://ned.usgs.gov/Ned/accuracy.asp [Accessed 31 March 2011].

van der Kamp, G., and Hayashi, M. 1998. *The groundwater recharge function of small wetlands in the semi-arid northern prairies.* Center for Great Plains Studies, Lincoln, NE. Report No. 8, pp. 39–56.

van Zyl, J. 1998. Unsupervised classification of scattering behavior using radar polarimetry data. *IEEE Transactions on Geoscience and Remote Sensing*, Vol. 27, No. 1, pp. 36–45. doi: 10.1109/36.20273.

Vymazal, J. 2005. Constructed wetlands for wastewater treatment. *Ecological Engineering*, Vol. 25, No. 5, pp. 475–477. doi: 10.1016/j.ecoleng.2005.07.002.